UC Davis
UC Davis Previously Published Works

Title

Collaboration of human pickers and crop-transporting robots during harvesting – Part I: Model and simulator development

Permalink
https://escholarship.org/uc/item/0j36x3fk

Authors
Seyyedhasani, Hasan
Peng, Chen
Jang, Wei-jiunn
et al.

Publication Date
2020-05-01

DOI
10.1016/j.compag.2020.105324

Peer reviewed

eScholarship.org Powered by the California Digital Library
University of California

Collaboration of Human Pickers and Crop-transporting Robots during Harvesting - Part I: Model and Simulator Development

Hasan Seyyedhasani[1,*], Chen Peng[1], Wei-jiunn Jang[1], and Stavros G. Vougioukas[1]

[1] Biological and Agricultural Engineering Department, University of California-Davis, One Shields Avenue, Davis, CA 95616
[*] Corresponding Author: Email: hshasani@ucdavis.edu; Tel.: +1 (859) 536 8233

ABSTRACT

Some specialty crops, such as strawberries and table grapes, are harvested by large crews of pickers who spend significant amounts of time carrying empty and full (with the harvested crop) trays. A step toward increasing harvest automation for such crops is to deploy harvest-aid robots that transport the empty and full trays, thus increasing harvest efficiency by reducing pickers' non-productive walking times. To that end, this work addresses human-robot collaboration modeling in a harvesting context. First, a modeling framework for all-manual and robot-aided harvesting was developed, which can be used for off-line simulation by system designers, but also as a representation model for robot control, during real-time operation. To serve both functions, the framework utilizes hybrid systems to model picker and robot activities. Finite state machines model discrete operating states, and difference equations describe motion and mass transfer within each discrete state. To capture the variability in human behavior and performance during harvesting, the human activity model utilizes stochastic parameters (e.g., picking time, walking speed) that can be estimated by measurements during harvesting. The stochastic model does not require direct yield measurements, which are not available for most specialty crops. Second, a stochastic simulator was developed based on the developed model. For a given field and crew size, the simulator samples all stochastic parameters to generate many instances of the harvest operation, and estimates metrics such as pickers' non-productive time and harvest operation efficiency. Part II of this work presents the calibration and evaluation of the simulator based on field data, and a case study that evaluates the effect of various robot scheduling algorithms on harvest efficiency.

Keyword: Specialty crops harvest mechanization; human-robot collaboration; stochastic modelling; harvest simulation.

1 INTRODUCTION

Mechanizing the hand harvesting of fresh market crops constitutes one of the biggest challenges to the sustainability of the fruit and vegetable industries. Depending on the commodity, labor for manual harvesting can contribute up to 60% of the yearly operating costs per acre (e.g. Bolda, Tourte, Murdock & Sumner, 2016). Additionally, recent studies indicate that the farm labor supply cannot keep up with demand in many parts of the world as a result of socioeconomic, structural and political factors (Bloomberg News, 2018; Z. Guan, Wu, Roka, & Whidden, 2015). Despite recent progress on shake-catch approaches for mechanical harvesting of apples (He et al., 2017) and cherries (Zhou et al., 2016), fruit quality and collection efficiency are still not adequate to justify adoption of these technologies for harvesting tree fruits. Shake-catch is also not applicable to the harvest of high-value crops like fresh strawberries, raspberries, blackberries, table grapes and tomatoes. These crops are very frail and must be harvested selectively, based on ripeness criteria, without inflicting damage. Robotic harvester prototypes are being developed and field-tested for high-volume, high-value crops such as apples (Silwal et al., 2017), kiwifruit (Williams et al., 2019), sweet pepper (Bac et al., 2017) and strawberries (Xiong, Ge, & Grimstad, 2019). However, the developed robots have not successfully replaced yet the judgment, dexterity and speed of experienced pickers at a competing cost; the challenges of achieving high fruit picking efficiency and throughput remain still largely unsolved (Bac, Henten, Hemming, & Edan, 2014; Silwal et al., 2017; Williams et al., 2019).

The manual harvesting operations for crops like strawberries, raspberries, blackberries, table grapes and tomatoes share a common feature: pickers spend significant amounts of (non-productive) time walking, to carry full and empty containers for the crops they pick. More specifically, during harvesting, each picker selects and picks the desired crops and places them in a small container (e.g., a basket, tray, bag or wheelbarrow). Once the container is full, the picker walks to a loading-inspection station at the edge of the field, waits in a queue, delivers the container with the harvested crops for inspection and compensation purposes, takes an empty container and walks back to resume picking. As a short or medium-term alternative to complete mechanization, teams of harvest-aiding robots are being developed that supply pickers with empty trays and transport full trays to collection stations (Vougioukas, Spanomitros, & Slaughter, 2012). Such robots can reduce walking, which often takes place on slippery ground, and consequently increase picker and harvest operation efficiency and safety.

Figure 1. a) Workers picking and transporting trays; b) robot prototype transporting a tray. Photos taken in a strawberry field in Salinas, CA, on August 1, 2017.

It is important to note that manual harvesting with robot-based transportation and the associated robot scheduling problem, resemble agricultural field operations, where several machines (Primary Units - PUs) perform the main field task (e.g., spraying, fertilizing, harvesting), and other machines (Service Units - SUs) provide in-field logistics support, by transporting working materials (crop, seeds, chemicals) between PUs and other units stationed outside the field (DD Bochtis & Sørensen, 2010). For example, pickers can be considered as grain harvesters (PUs), personal crop containers (tray, bag) as harvester grain tanks, and robots as transport trucks (SUs); of course, manual harvesting rates vary among workers in non-deterministic ways and are very difficult to measure in the field. Simulation models have been developed to study field machine operations. Arjona, Bueno, and Salazar (2001) used a discrete event simulation model to study the processes of harvesting and transporting sugarcane. De Toro and Hansson (2004) simulated in-field machinery performance for a series of years using a discrete events approach. Dionysis Bochtis, Vougioukas, Ampatzidis, and Tsatsarelis (2007) developed a hierarchical modeling framework for field operations planning of a fleet of machines. S. Guan, Nakamura, Shikanai, and Okazaki (2008) introduced hybrid modelling to simulate farm work planning and applied it to sugarcane farming. Hameed, Bochtis, Sørensen, and Vougioukas (2012) developed an object-oriented simulation model to evaluate machinery activities that involve transport and application of inputs (e.g., seeds, fertilizers, chemicals) in fields. Zhou, Jensen, Bochtis, and Sørensen (2015) modeled the sequential operations of rotation farming (e.g., planting, spraying and harvesting) to predict the performance of potato production operations.

Although machine field activity modelling has been pursued by many researchers, the modelling of manual harvesting has not received as much attention. Researchers have shown that simulation models can improve greenhouse operations (Van Henten, Bac, Hemming, & Edan, 2013). Bechar, Yosef, Netanyahu, and Edan (2007) modelled manual tomato trellising and harvesting operations in greenhouses using an event-based approach; simulated changes in work practices yielded up to 32% improvements. Van't Ooster, Bontsema, van Henten, and Hemming (2012) developed a discrete event simulator to model worker actions in a rose cultivation system inside greenhouses. They used the model to determine the best system settings at given rose yield levels and increase labor efficiency. The model was also used for static cut rose cultivation system (van't Ooster, Bontsema, van Henten, & Hemming, 2015) and sweet pepper harvesting operations (Elkoby, van't Ooster, & Edan, 2014). All the work cited above addressed protected cultivation environments – not open fields- and yield distribution was assumed to be a known input to the models, because measurements of yield were possible using greenhouse worker tracking systems (e.g., rose stems per m^2). Unfortunately, yield distributions are not available for open-field, manually harvested specialty crops. Also, the above works modeled only manual labor and did not incorporate any machine operations, or human-machine interactions. A few works have modeled workers actions during open-field harvest operations. Ampatzidis, Vougioukas, Whiting, and Zhang (2014) adopted a queueing model from operations research to describe the fruit picking process in sweet cherry harvest and the bin loading process in table grape harvest. Mesabbah, Mahfouz, Ragab, and Arisha (2016) developed a hybrid model, consisting of discrete event simulation and agent-based modeling to study the effect of varying performance of human harvesters in the productivity and operational cost of vineyard harvesting operations. Again, the researches cited above modelled manual activities only, and did not incorporate machine operations or collaboration between pickers and machines. Also, all cited modeling approaches could be used only for simulation and were not suitable as task models for robot control purposes, in the context of human-robot collaboration. As identified by Sheridan (2016) and others, humans need a mental model of the robot's capabilities and vice versa—also robots need to understand human actions and reactions.

Hence, to the best of our knowledge, models that describe the collaboration of robots and humans during open-field specialty crop harvesting without explicit knowledge of yield spatial distribution, and that can be used for simulation and robot control purposes have not been studied yet. Motivated by the above mentioned challenges and limitations, the major contribution of this work is the development of a novel approach that utilizes hybrid automata with stochastic parameters to model the all-manual and robot-aided harvest and crop-transport operations for specialty crops that involve picking and walking. The developed models are suitable for simulation and robot control, and are based on parameters which can be estimated from measurements that can be made in real harvesting conditions; knowledge of crop yield maps (which are actually not available for manually harvested crops) and human picking rates (which are stochastic, time varying and extremely difficult to measure) are not required. Additionally, based on the presented methodology, a simulator was developed to predict picking efficiencies of a picking crew in harvesting operations for specialty crops and to evaluate various scheduling and dispatching policies for robot teams of different sizes serving the picking crew.

The rest of this paper is organized as follows: Section 2 describes the manual and robot-aided harvesting processes for specialty crops that require picking and transport. In Section 3 and 4, a methodology is presented that uses multiple interacting stochastic hybrid automata to model manual picking and robot crop transport operations, and their interactions. Then the implementation of a simulator is presented that is based on the developed methodology. Lastly, the work in concluded, in Section 5, by discussing how useful the developed model can be for in harvest-aid robotics.

2 Manual Harvesting without and with Crop-Transporting Robots

In California and other parts of the world, soft-fruit crops such as strawberries, raspberries, table grapes and fresh tomatoes are typically planted in equally spaced parallel rows with furrows/aisles between them that accommodate human and machine traffic (Figure 2).

Figure 2. Layout of a typical raised-bed strawberry field (left) and vineyard (right) (AFP, 2013).

The field headlands are reserved for collection/packing/inspection stations and traffic of people, forklifts and trucks involved in the handling and transportation of the harvested crop. Strawberry harvesting will be used as an example in the rest of this paper; however, the methods and approaches are applicable for any manually harvested crops that require picking and transport.

The size of the picking crew ranges from 15-20 pickers (for smaller fields) to 35-40 pickers (for larger fields). Furrows can be quite long (up to 100 m). Picking starts from one corner of a field block, and advances towards the other corner. Each picker enters a furrow and starts picking strawberries selectively from the plants on the raised beds on each side of that furrow. Plucked strawberries are placed in a carton container called a ‘tray’ or ‘flat’; fresh-market strawberries are actually placed in small plastic containers (aka clamshells) inside the tray. The tray lies on a small ‘picking cart’ that is essentially a wheelbarrow made of wire (Figure 3).

Figure 3. A picker is picking and placing strawberry into a tray, carried by a cart, while in a furrow. Photo taken in a strawberry field in Salinas, CA, on August 1, 2017.

At any time during picking, the worker may pause due to fatigue or the need for personal time. The picker moves forward and continues picking until the tray is full. This may happen inside the furrow the picker has been working in, or, if all fruit reachable from that furrow has been picked, in another furrow. In the former case, the picker leaves the cart where (s)he stopped picking, and walks to carry the tray to the collection station. In the latter case, the picker exits the current furrow, walks along the field’s headland, carrying the cart with them, and enters the next empty furrow (no one else has used it) to harvest the next non-harvested bed. Once a tray is full it must be transported to the collection station. To reduce transport time, each block is split into two sections which also mark the center of furrows; so pickers typically start picking from the beginning of a section (the center of each furrow) and advance towards the headland where the collection station is located. After one section of the field is harvested, the collection station is moved to the opposite headland and the other section is harvested. Additionally, in some cases (when a field is very wide) there may be more than one collection stations dispersed along the headland that are manned – and become active – progressively as the crew sweeps the field from left to right, or vice versa. If crop-transport automation is not available, pickers must walk and bring their filled trays to a collection station, wait for quality inspection, register their tray for compensation, and get an empty tray to return to the field and resume picking (Figure 4).

Figure 4. Pickers wait in a queue at a collection station to register their tray.

In the proposed robot-aided harvesting scheme, a team of identical small robots brings empty trays to pickers and transports their full trays to the collection station. Robot are small, so they can carry only one tray, and tray loading and unloading is done manually. At any given time, given a set of tray-transport requests and a number of idle robots at the collection station, a scheduling/dispatching module schedules and dispatches robots to pickers. A dispatched robot departs from the collection station and carries an empty tray to the designated picker; when the robot arrives, the picker exchanges the filled tray with the empty tray and resumes picking. The robot carries the filled tray back to the collection station where someone takes the full tray and loads an empty one. Given that the number of robots will be small, this work assumes that robots don't wait in a queue at the collection station. The job cycle continues until all trays have been harvested and transported. Hence, non-productive walking time (traveling to a collection station) and waiting in a queue is eliminated. However, since robots are shared, pickers may have to wait for a robot to arrive.

3 Modelling Challenges and Overview of Proposed Approach

To reduce cost, each robot should serve multiple pickers. That is, the robot team is a shared resource; so the robot deployment will introduce a *waiting time*, t_{wait}, for each transported container. This is non-productive time, Δt_{fe}, during which a picker waits for a robot to arrive, after (s)he has filled their personal container. Clearly, reducing non-productive walking will cause Δt_{fe} to decrease, but the waiting time will cause it to increase. Therefore, proper/optimal scheduling of robot teams, in real-time, is essential to minimize waiting times and equivalently maximize labor savings and efficiency, in a cost-effective manner.

Computing the distributions of waiting times and efficiencies of different robot scheduling algorithms, and comparing them with all-manual harvesting, for different harvest scenarios (field size, crop load, picking crew size and characteristics) and robot teams (size, operating speeds, and capacities) is extremely important for designing cost-effective robotic crop-transport systems. Such prediction requires validated models and simulators of all-manual and coupled human-robot operations. More specifically, the location and time when each picker fills up each of their container and the time it takes to transport it manually and return must be computed, along with the waiting time a picker waits for a robot to arrive, in robot-aided operation. Therefore, the goals of this paper are: to present a modelling framework for the coupled operations of manual harvesting and robot-aided crop transport, for specialty crops whose harvest requires workers to pick and deliver; and to present a stochastic simulator based on the proposed model that can be used to predict picking efficiencies for a crew of pickers, and evaluate various scheduling strategies for teams of harvest-aid transport robots.

At the very core of the manual harvesting model lies the calculation of the position of a picker and the amount of crop harvested by the picker as functions of time. A picker's current path, *c*, depends on what (s)he is doing, i.e., an operating state/mode: when picking, the path is a straight line inside a furrow; when delivering a tray it is typically a straight line segment from the exit point of the current furrow to the collection station; when moving to the next unharvested row, it is the line segment between the current furrow's exit and the next furrow's entry point. Hence, it is assumed that all travel paths are known in advance. A picker's position $d(t)$ on a predefined path *c*, is the line integral of the picker's instantaneous moving speed, $v(t)$ (m s^{-1}), along this path:

$$d(t) = \oint_{t_0}^{t_0+\Delta t} v(\tau)d\tau \qquad (1)$$

The moving speed depends on the individual picker and on what (s)he is doing (e.g., picking, carrying a tray, waiting); it will also typically vary with time, and depend on other random factors. From the above, it becomes clear that a harvesting model must have a *discrete* aspect, which represents different 'operating states', and a *continuous* aspect, for worker position integration. It would also not be practical to develop models that rely on knowledge of workers' moving speed profiles along paths to calculate worker positions.

The picking operating state is of particular importance. When picking fruit from plants along a straight-line path *c* inside a furrow, the moving speed depends strongly on the yield, $y(c)$ (kg m^{-1}), along the path, and on the worker picking rate, $p(t)$, (kg s^{-1}). High yields result in slow moving speeds because the picker must collect a lot of fruit at the same or nearby locations, whereas high picking rates result in high moving speeds, since all harvestable fruit at the same or nearby locations is picked quickly. If yield distribution and picking rate were known, moving speed could be calculated as:

$$v(t) = \frac{p(t)}{y(c(t))} \qquad (2)$$

However, yield distributions are not available for specialty crops – even from historical data - because they are harvested manually, and harvest monitors that measure yield are not available. Also, picking rates vary among workers (e.g., due to age, physical ability); are time-varying (e.g., due to fatigue, psychological condition); stochastic (e.g., sudden pauses for personal reasons) and very difficult to measure in the field. Calculating the weight of harvested fruit in the tray at time *t,* $W(t)$, also requires that the picking rate is known:

$$W(t) = \oint_0^t p(\tau)d\tau \quad (3)$$

Furthermore, knowing the amount of time required for a tray to fill up, Δt_{ef}, is necessary for modelling purposes, because it specifies the time and location of the next tray transport request (upper limit of integration in equation (3)). If a worker starts filling up an empty tray at some position inside a furrow at time 0, one could compute the time Δt_{ef} by solving the equation shown above for $w(\Delta t_{ef}) = W_{full}\text{-}W_{empty}$, i.e., when the tray becomes full (since the tray's capacity and empty weight are known). Unfortunately, the picking rate is not known and therefore Δt_{ef} cannot be calculated.

For all the above reasons, manual harvesting models that assume that the yield and picking rate parameters are available are not practical. To address this problem, the following approach is adopted in this work.

1) Hybrid automata are used to model the discrete and continuous activities taking place during manual and robot-aided harvesting.

2) The picker mean moving speeds during all different harvest activities, the time needed to fill-up trays Δt_{ef}, and the idle time spent waiting at the collection station, Δt_{iq}, are modelled as stochastic parameters with distributions that are approximated from frequency histograms identified from measurements of these parameters during the corresponding field harvest activities.

3) Monte-Carlo simulation is used to sample the corresponding stochastic parameters for each picker and for each harvested and delivered tray, and to estimate the distributions of waiting times t_{wait}, and non-productive times Δt_{fe}, so that efficiency metrics can be predicted.

Since the picking time Δt_{ef} is known (from measurements) the mean picking rate that is consistent with equation (3) is computed from the mean value theorem and used in equation (3) to simulate fruit picking, assuming constant picking rate. The mean moving speed $\bar{v}$ during picking is modelled directly, without the need to know picking rates and yields. Again, because of the mean value theorem, $\bar{v}$ and Δt_{ef} can be used in equation (1) to update worker position and compute the location along the furrow $d(\Delta t_{ef}) = \bar{v}\,\Delta t_{ef}$ where the tray will fill-up. Next, the developed modelling framework will be presented in detail.

4 METHODOLOGY

4.1 WORKSPACE MODELLING

In a field with F furrows, each furrow is given a unique number/index, f $(1 \leq f \leq F)$. The point in the middle of furrow f - along its length - is the 'split-point' $(x_s(f),\ y_s(f))$. The line through the split-points of all furrows divides the field block into two sections, which are harvested in sequence. Each section has an index, denoted as sec, that is equal to one or zero for 'upper' or 'lower' block section, respectively. The end-point of a furrow, f, in section, sec, is represented by coordinates $x_e(f, sec),\ y_e(f, sec)$, and represents the border between the furrow and the headland: pickers and robots enter and exit the furrow via the end-point. The point inside a furrow where a picker stops picking because the tray filled up (and from where the picker will resume harvesting) is denoted as $x_b(f, sec),\ y_b(f, sec)$. For brevity, the dependence on (f, sec) will not be shown in the rest of the text, except where necessary. Finally, the position of the collection station is denoted as (x_{cs}, y_{cs}). All the above points are used as nodes in a graph that models field coverage as graph traversal (DD Bochtis, Vougioukas, & Griepentrog, 2009; Seyyedhasani & Dvorak, 2017).

4.2 MODELLING OF MANUAL AND ROBOT-AIDED HARVESTING

Discrete-time hybrid systems/automata are adopted as a unified approach to model the activities, motions and interactions of all agents - human pickers and robots - involved in harvesting. Finite State Machines

(FSMs) are used to model the discrete operating states/modes of the agents and the transitions between states, whereas difference equations describe motion and mass (crop) transfer inside each operating state. Hybrid automata were originally proposed as an approach to the control of complex motion control systems and robots (Brocket, 1993; Huber & Grupen, 1996), because of their ability to implement reactive control (continuous domain) in a task-dependent fashion (discrete domain). It is also known that complex robotic "behavioral procedures" (Arkin, 1998) can be modeled formally using hybrid automata (Egersted, 2000). Discrete-time dynamic systems offer a powerful and flexible approach that has been used for more than 60 years to describe and analyze the dynamics of human–machine systems, when a human operator acts as manual controller (Rouse and Gopher, 1977). Hybrid automata have been proposed to model more complex human behavior in the context of dynamically coupled man-machine cooperative systems such as power-assist mechanisms (Okuda et al., 2007). In this work, hybrid automata were used to model both human and robotic "behaviors" during harvest. There are, of course, other ways to model/program behaviors (e.g., arbitrating or fusing independent reactive control actions or rules (Arkin, 1998)). However, in the context of harvesting, picker "behavior" and interaction with robots via tray exchange depends on yield and other factors, such as picker physical and psychological state, random work interruption for personal time. Hybrid automata enable the modeling of human pickers' actions using stochastic parameters and variables (e.g., walking speed, time to fill a tray) that can be measured in the field, so that the model and simulator can be calibrated and validated. Furthermore, hybrid automata models can be used for simulation - off-line - and for robot control, online.

At any discrete time k, each agent α ($a \in \{p, r\}$ for picker and robot) involved in the harvesting process is in a discrete operating mode/state s_a^i. The agent has also a continuous state, $\boldsymbol{X_{a,k}} = (\mathrm{x}_{a,k}, \mathrm{y}_{a,k}, W_{a,k}, T_{a,k})$ with known initial conditions $\boldsymbol{X_{a,0}}$. The continuous state variables are: the agent's position coordinates x, y in the world frame; the weight W of the agent's tray, and the elapsed time T inside the current state s_a^i. In state s_a^i the continuous state is governed by discrete state-dependent difference equations of the form:

$$\mathrm{x}_{a,k+1} = \mathrm{x}_{a,k} + \Delta t \cdot V_{s_a^i} cos(\theta), \tag{4}$$

$$\mathrm{y}_{a,k+1} = \mathrm{y}_{a,k} + \Delta t \cdot V_{s_a^i} sin(\theta), \tag{5}$$

$$\mathrm{W}_{a,k+1} = \mathrm{W}_{k} + \Delta t \cdot p_{s_a^i}, \tag{6}$$

$$T_{a,k+1} = T_{a,k} + \Delta t. \tag{7}$$

$V_{s_a^i}$ is the agent's moving speed, θ is the direction of motion, $p_{s_a^i}$ is the agent's picking rate, and Δt is a discrete time step; all quantities with a subscript s_a^i depend on the operating state. The initial conditions are $\mathbf{X}_{a,0} = \left[\mathrm{x}_{s_a^i,0}, \mathrm{y}_{s_a^i,0}, \mathrm{W}_{s_a^i,0}, t\right]$. In this work, the agents are assumed to have single-integrator dynamics for position (Eqs. 4 and 5) and zero-order dynamics for speed V and direction θ (they can change instantaneously). Such simplified modeling of dynamics is common for planning and analyses of teams of agents (Gazi et al., 2015). Furthermore, during manual harvesting in long rows (like our scenarios), the large majority of motions are straight-line motions along furrows – and fewer motions in headlands - at constant speeds. Therefore, changes in speed and direction take place only at the (short-lasting) transitions when an agent crosses furrow and headland. Therefore, any differences in the simulated tray transport times from the simplified dynamics are not expected to be significant. At the next time step the agent may remain in s_a^i or transition to another discrete state s_a^j; the transition is denoted as $(\boldsymbol{X}_{a,k}, s_a^i, s_a^j)$. State transitions are either deterministic or stochastic. Next, models are presented for the operations of a single picker, a group of pickers, a group of independent robots, and collaborating pickers and robots.

4.2.1 Single Picker Manual Picking Model

Finite State Machine for picker operating modes

The activities of a picker during manual harvesting can be grouped in nine *discrete operating states* (Table 1). These states are: $s_p^i \in$ {START, IDLE-IN-QUEUE, WALK-EMPTY-TRAY-HEADLAND, WALK-EMPTY-TRAY-FURROW, PICKING, WALK-TO-NEXT-FURROW, SETUP, TRANSP-FULL-TRAY-FURROW, TRANSP-FULL-TRAY-HEADLAND, STOP}.

Table 1. States defined to represent a picker's actions during manual harvesting.

S_p	State	Action
s_p^0	START	A picker with an empty tray in hand starts harvesting.
s_p^1	IDLE-IN-QUEUE	A picker waits in a line at the collection station to deliver her/his full tray, and receive an empty tray.
s_p^2	WALK-EMPTY-TRAY-HEADLAND	A picker walks in the headland - toward a furrow - carrying an empty tray, to continue harvesting.
s_p^3	WALK-EMPTY-TRAY-FURROW	A picker with an empty tray walks inside a furrow toward its split-point to either harvest the furrow for the first time or continue harvesting in it.
s_p^4	PICKING	A picker is picking inside a furrow, with direction from its split-point toward the headland.
s_p^5	WALK-PARTLY-FULL-TRAY-HEADLAND	After finishing a bed, if the tray is still not full, the picker walks in the headland toward an empty furrow (no one has used it) to harvest the next non-harvested bed.
s_p^6	WALK-PARTLY-FULL-TRAY-FURROW	A picker with a partially full tray walks inside an empty furrow – until its split-point is reached – to continue harvesting from an unharvested bed.
s_p^7	TRANSP-FULL-TRAY-FURROW	A picker walks inside a furrow toward the headland to transport the full tray to the collection station.
s_p^8	TRANSP-FULL-TRAY-HEADLAND	A picker walks in headland to transport the full tray to the collection station.
s_p^9	STOP	A picker stops picking after delivering the last tray.

The states and possible transitions are shown in Figure 5. For brevity, same-state transitions are not shown, as all the states continuously transition to themselves until a transition condition to another state is satisfied.

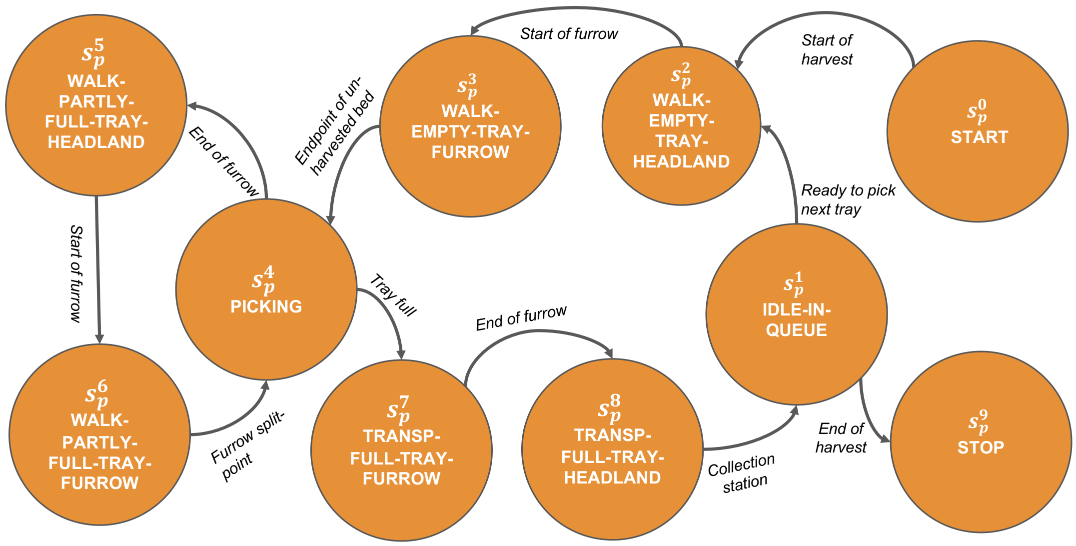

Figure 5. State diagram of a picker's operating states/modes (s_p^i) during manual strawberry harvesting.

START

In state s_p^0, the picker with an empty tray in hand starts the harvesting operation. The state initial conditions are $\mathbf{X}_{p,0} = [\mathrm{x}_{cs}, \mathrm{y}_{cs}, \mathrm{W}_{empty}, 0]$, where $(\mathrm{x}_{cs}, \mathrm{y}_{cs})$ is the position of the collection station, and W_{empty} is the weight of an empty tray. The transition "*Start of harvest*" takes place immediately, i.e., no integration is performed.

IDLE-IN-QUEUE

In state s_p^1, the picker waits in the queue at the collection station, delivers the full tray and gets an empty tray. The picker stays in this state for Δt_{iq} (s). The pdf of Δt_{iq} is approximated from a frequency histogram identified from measurements. The initial condition for the continuous states is $\mathbf{X}_{p,0} = [\mathrm{x}_{cs}, \mathrm{y}_{cs}, \mathrm{W}_{full}, \mathrm{t}]$, where W_{full} is the weight of a full tray (including the empty tray's weight). The fact that the picker leaves with an empty tray is modeled by using a 'picking rate' $p_{s_p^1} = (W_{empty} - W_{full})/\Delta t_{iq}$., The picker moving speed is $V_{s_p^1} = 0$. As soon as $T_{p,k} - T_{p,0} \geq \Delta t_{iq}$, if there are still unharvested beds the "*Ready to pick next tray*" transition, s_p^1 to s_p^2, takes place; otherwise, the "*End of harvest*" transition to the "STOP' state s_p^9 takes place.

WALK-EMPTY-TRAY-HEADLAND

In state s_p^2, the picker walks in the headland, from the collection station toward the 'end-point' of a furrow. This furrow is the closest un-occupied furrow that has not been traversed yet for harvesting (see section 4.2.2 for the furrow selection process), or the furrow the picker was already working in. The travel angle θ is defined by the straight line connecting the collection station and the target furrow's end-point x_e, y_e, and corresponds to a direction away from the collection station. The state initial conditions are: $\mathbf{X}_{p,0} = [\mathrm{x}_{cs}, \mathrm{y}_{cs}, W_{full}, t]$. The picker walking speed $V_{s_p^2} = V_W$, a random variable whose pdf is approximated from a frequency histogram identified from measurements, and the picking rate $p_{s_p^2} = 0$. The "*Start of furrow*" transition, s_p^2 to s_p^3, takes place when a picker reaches the end-point of the furrow.

WALK-EMPTY-TRAY-FURROW

In state s_p^3, a picker with an empty tray walks inside a furrow toward its middle to either harvest it for the first time or continue harvesting in it. The initial conditions are $\mathbf{X}_{p,0} = [\mathrm{x}_e, \mathrm{y}_e, W_{empty}, t]$. The picker's walking speed is $V_{s_p^4} = V_W$ and the travel angle θ is the heading of the furrow with direction toward its split-point $(\mathrm{x}_s,\ \mathrm{y}_s)$. The picking rate is $p_{s_p^4} = 0$. The transition "*Endpoint of un-harvested bed*" from s_p^3 to s_p^4 (picking state) takes place as soon as the picker reaches the split-point (if the furrow is entered for the first time) or the location in the furrow where the previous tray had been filled, i.e., the boundary between harvested and un-harvested crop $(\mathrm{x}_b,\ \mathrm{y}_b)$.

PICKING

In state s_p^4, the picker picks inside a furrow, with direction from its split-point toward the headland. If this furrow was entered for the first time the initial coordinates are the furrow's split-point $(\mathrm{x}_s,\ \mathrm{y}_s)$, and if the previous state was s_p^3 (carrying an empty tray), then the initial weight is $\mathrm{W}_{s_p^4,0} = W_{empty}$; otherwise, the previous state was s_p^6 (carrying a partially full tray), and the initial weight is the weight of partially full tray, $\mathrm{W}_{s_p^4,0} = W_{partial}$. If the picker was picking in this furrow before, the initial position is $(\mathrm{x}_b,\ \mathrm{y}_b)$ and corresponds to the point where the previous tray had filled up, and $\mathrm{W}_{s_p^4,0} = W_{empty}$. The picker walking speed is $V_{s_p^5} = V_P$, a random variable whose pdf is approximated by a frequency histogram identified from measurements during picking from a furrow. The travel angle θ is the heading of the furrow with direction toward the headland. The process of filling one tray lasts Δt_{ef} seconds. This time interval is a random variable (Anjom et al., 2018) whose pdf is approximated by a frequency histogram identified from measurements. The picking rate is $p_{s_p^5} = (W_{full} - W_{empty})/\Delta t_{ef}$. If the time spent picking $(T_{p,k} - t)$ exceeds Δt_{ef} before the picker reaches the end-point of the furrow, the transition "*Tray full*" takes place from s_p^4 to s_p^8, and the picker begins transporting the full tray. However, if the end of the furrow is reached before Δt_{ef} is exceeded, the "*End of furrow*" transition occurs from s_p^4 to s_p^5, and the picker walks to the next empty furrow to continue picking and filling the same tray.

WALK-PARTLY-FULL-TRAY-TO-NEXT-FURROW

After harvesting a bed, if the tray is partly full, the picker enters state s_p^5, where (s)he walks in the headland toward the closest un-occupied furrow that has not been used yet. During walking, the picker carries the partly full tray and the picking cart. The initial conditions are $\mathbf{X}_{p,0} = [\mathrm{x}_{fe},\ \mathrm{y}_{fe}, W_{partial}, \mathrm{t}]$. The picker walking speed is $V_{s_p^6} = V_T$, a random variable whose pdf is approximated by the frequency histogram identified from measurements. The travel direction θ is defined from $(\mathrm{x}_e(f, sec),\ \mathrm{y}_e(f, sec))$ of the current furrow, *f*, to the end-point of the next furrow, *f'*, $(\mathrm{x}_e(f', sec),\ \mathrm{y}_e(f', sec))$; the picking rate is $p_{s_p^6} = 0$. The "*Start of furrow*" transition, s_p^5 to s_p^6, occurs when a picker reaches $(\mathrm{x}_e(f', sec),$ $\mathrm{y}_e(f', sec))$.

WALK-PARTLY-FULL-TRAY-FURROW

In state s_p^6, a picker carrying a partly-full tray walks in a furrow toward – and until - its split-point. The initial condition for the continuous states is $\mathbf{X}_{p,0} = [(\mathrm{x}_e(f', sec),\ \mathrm{y}_e(f', sec)), \mathrm{W}_{partial}, \mathrm{t}]$. The picker walking speed is $V_{s_p^6} = V_T$ and the travel angle θ is the heading of the furrow with direction toward the headland. The picking rate is $p_{s_p^7} = 0$. The transition from s_p^6 to s_p^4 occurs once the picker reaches the furrow's split-point $(\mathrm{x}_s,\ \mathrm{y}_s)$.

TRANSP-FULL-TRAY-FURROW

In state s_p^7 the picker walks inside the furrow toward the collection station to deliver the full tray. The state initial conditions are $\mathbf{X}_{p,0} = [\mathrm{x}_b, \mathrm{y}_b, \mathrm{W}_{full}, \mathrm{t}]$. The walking speed is $V_{s_p^7} = V_W$ and the travel angle θ is the heading of the furrow with direction toward the headland. The picking rate is $p_{s_p^8} = 0$. The "*End of furrow*" transition, s_p^7 to s_p^8, occurs when the picker reaches the furrow's end-point $(\mathrm{x}_e, \mathrm{y}_e)$.

TRANSP-FULL-TRAY-HEADLAND

In state s_p^8, the picker walks in headland to transport the full tray to the collection station. The state initial conditions are $\mathbf{X}_{p,0} = [\mathrm{x}_e,\ \mathrm{y}_e\ , \mathrm{W}_{full}, \mathrm{t}]$. The walking speed is $V_{s_p^9} = V_W$, and the angle θ is the travel direction in the headland. The picking rate is $p_{s_p^9} = 0$. The "*Collection station*" transition s_p^8 to s_p^1, occurs when the picker arrives at the collection station, at the point $(\mathrm{x}_{cs}, \mathrm{y}_{cs})$.

STOP

In state s_p^9, the picker stops harvesting, after having delivered the last tray to the collection station. The state initial conditions are $\mathbf{X}_{p,0} = [\mathrm{x}_{cs},\ \mathrm{y}_{cs}\ , 0, \mathrm{t}]$ and the time clock stops. This may happen before a lunch break, at the end of the day, or for other reasons.

4.2.2 Multi-Picker Crew Operation Model

Harvest crews consist of large numbers of pickers (15-30). Pickers harvest independently of each other; however, each furrow is typically traversed/occupied by only one picker. When harvest begins, each picker selects the closest furrow to that is unoccupied as the first furrow to work in; let its index be f(1). When the picker finishes harvesting from furrow f(1), (s)he moves to the next closest unoccupied furrow that corresponds to an unharvested bed (the index is f(2)). This process continues (f(3), f(4)…), until the entire field section is harvested; then, the whole crew transitions to the other section of the field. Through this process, a picker's choice of the next bed to harvest – and the corresponding furrow to walk in – restricts the selection of furrows by other pickers. The simulator models this interaction (i.e., coordination among the crew) by implementing for each picker the furrow transition pattern described above, and ensuring that a furrow visited by a picker is not available for another picker.
There are, however, a few exceptions to the typical traversal pattern: 1) if a tray becomes full while only a small length of the bed remains unharvested, a picker may harvest the remaining distance by overfilling the clamshells in the tray; 2) when a tray is almost full at the end of a bed/furrow, a picker may pick some strawberries from neighboring beds; and 3) if the tray is more than half-full when a picker enters a new furrow, the picker may choose to start harvesting from the entry point of the furrow rather than walking to its center first and then start picking. Including these exceptions in the model is possible, albeit at the cost of increased complexity. However, estimating their statistics is very difficult, as they don't happen often and depend on picker random/subjective decisions, habits, fatigue. Extensive observation of pickers confirmed that these exceptions are sporadic and as such would not affect the calculation of picking efficiency. Hence, they were not modeled in the developed system.

4.2.4 Integrated Human-Robot Harvesting Model

During human-robot collaborative harvesting, the pickers don't walk to the collection station to deliver full trays; they do so only once, for their last tray of the day. The operation of the transport-robots introduces two new picker states (Table 2). The state diagram of pickers and robots carrying trays is shown in Figure 6. Pairs of robot and picker state transitions that are mutually dependent have underlined text and same color.

Table 2. New picker states introduced for collaboration with crop-transport robots.

S_p	State	Action

s_p^{10}	WAITING-FOR-ROBOT	A picker with a full tray waits (idle) for a robot to arrive.
s_p^{11}	TRAY-LOADING	A picker takes the empty tray brought by the robot and places a full tray on the robot.

WAITING-FOR-ROBOT

In state s_p^{10}, the picker has filled a tray and waits for a robot to arrive. The initial conditions are $\mathbf{X}_{p,0} = [\mathrm{x}_{fb}, \mathrm{y}_{fb}, \mathrm{W}_{full}, \mathrm{t}]$. The picking rate $p_{s_p^{10}}$ and picker moving speed $V_{s_p^{10}}$ are zero. The "*Robot arrived*" transition, s_p^{10} to s_p^{11}, takes place when a robot arrives, i.e., the robot's "*Picker location*" condition (and transition) becomes true. Obviously, if the robot is already there, the picker exits this state immediately.

TRAY-LOADING

In state s_p^{11}, the picker takes the empty tray brought by the robot and places a full tray on the robot. The initial conditions are $\mathbf{X}_{p,0} = [\mathrm{x}_b, \mathrm{y}_b, \mathrm{W}_{full}, \mathrm{t}]$. The picking rate $p_{s_p^{10}}$ and picker moving speed $V_{s_p^{10}}$ are zero. The duration of this state is assumed constant and equal to some 'handling time' Δt_h. Tray handling is modeled with a picking rate $p_{s_r^4} = (W_{full} - W_{empty})/\Delta t_h$, which results in switching from a full to an empty tray ($\mathrm{W}_{r,k} = W_{full}$) when the state is exited. The "*Empty tray from robot*" transition, s_p^{11} to s_p^4, takes place once $T_{p,k} \geq t + \Delta t_h$.

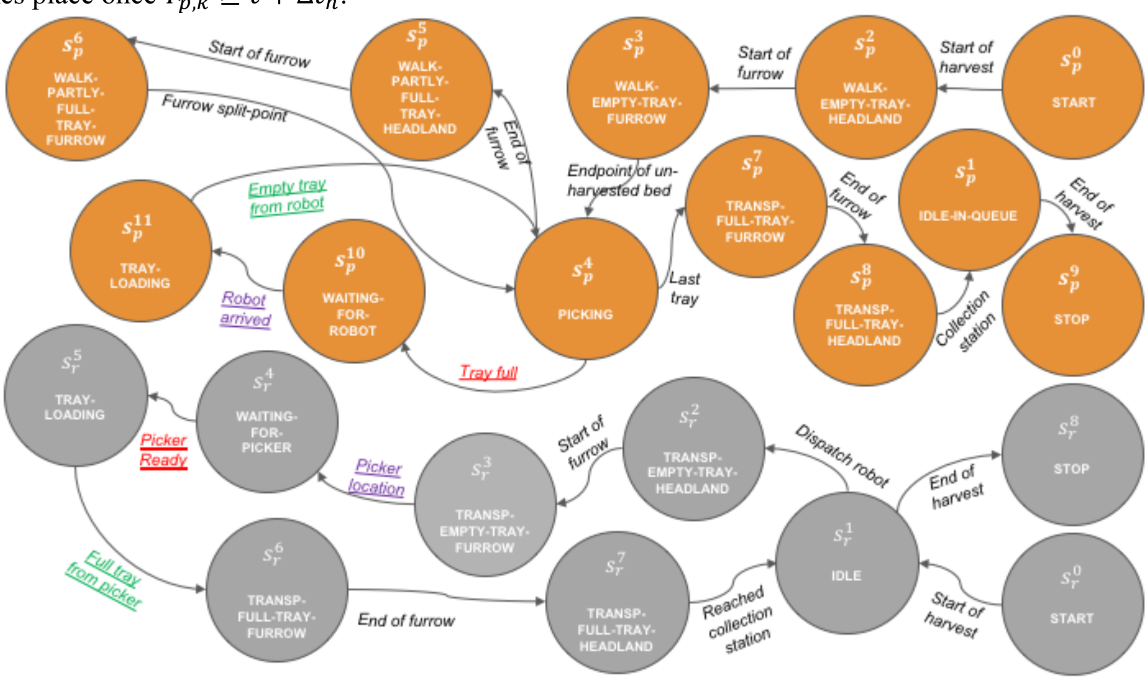

Figure 6. State diagram of picker states (s_p^i) and transport robot states (s_r^i) during human-robot collaborative harvesting, where robots carry empty and full trays between pickers and the collection station.

As with picker actions, the operations of a crop-transport robot can be grouped in discrete operational states (Table 3): $s_r^i \in$ {START, IDLE, TRANSP-EMPTY-TRAY-HEADLAND, TRANSP-EMPTY-TRAY-FURROW, TRAY-LOADING, TRANSP-FULL-TRAY-FURROW, TRANSP-FULL-TRAY-HEADLAND, STOP}.

Table 3. States defined to represent robot actions during the tray transportation

s_r	State	Action

s_r^0	START	A robot at the collection station starts operation with no tray on it.
s_r^1	IDLE	Robot remains idle until dispatched to a picker.
s_r^2	TRANSP-EMPTY-TRAY-HEADLAND	Robot travels in the headland - carrying an empty tray - toward the end-point of the furrow where the service request originated.
s_r^3	TRANSP-EMPTY-TRAY-FURROW	Robot travels inside a furrow - carrying an empty tray - toward the location where the transport request originated.
s_r^4	WAITING-FOR-PICKER	The robot waits until the picker fills her/his tray.
s_r^5	TRAY-LOADING	The robot is still while the picker exchanges the empty tray with a full tray.
s_r^6	TRANSP-FULL-TRAY-FURROW	Robot travels inside a furrow - carrying a full tray - toward the collection station.
s_r^7	TRANSP-FULL-TRAY-HEADLAND	Robot travels in the headland - carrying a full tray - toward the collection station.
s_r^8	STOP	The robot at the collection station stops its harvest-aid operation after transporting the last tray.

A robot's operating modes are described next:

START

In state s_r^0, the robot is at the collection station with an empty tray on it, and starts its operation. The initial conditions are $\mathbf{X}_{p,0} = [\mathrm{x}_{cs}, \mathrm{y}_{cs}, \mathrm{W}_{empty}, 0]$. The transition "*Start of harvest*" takes place immediately.

IDLE

In state s_r^1, the robot remains idle (waits) at the collection station. If this state is entered for the first time from the START state, the initial tray weight is $\mathrm{W}_{init} = \mathrm{W}_{empty}$; otherwise, $\mathrm{W}_{init} = \mathrm{W}_{full}$. The initial conditions are $\mathbf{X}_{r,0} = [\mathrm{x}_{cs}, \mathrm{y}_{cs}, \mathrm{W}_{init}, \mathrm{t}]$. The picking speed is $p_{s_r^1} = (W_{empty} - W_{init})/\Delta\mathrm{t}$, and its moving speed is zero. If there are still requests for tray transportation the "*Dispatch robot*" transition, s_r^1 to s_r^2 is initiated by the scheduling/dispatching module; otherwise, the "*End of harvest*" transition to the "STOP' state s_r^8 takes place.

TRANSP-EMPTY-TRAY-HEADLAND

In state s_r^2, the robot travels in the headland - carrying an empty tray – toward the end-point of the next furrow, $(\mathrm{x}_e,\ \mathrm{y}_e)$, which is specified by some scheduling algorithm. The initial conditions are $\mathbf{X}_{r,0} = [\mathrm{x}_{cs}, \mathrm{y}_{cs}, \mathrm{W}_{empty}, \mathrm{t}]$. The robot speed is constant and pre-set at $V_{s_r^2} = V_r$; θ is defined by the collection station and furrow end-point locations, with direction toward the furrow. The picking rate is zero. The "*Start of furrow*" transition, s_r^2 to s_r^3, takes place when the robot reaches the end-point of the furrow $(\mathrm{x}_e, \mathrm{y}_e)$.

TRANSP-EMPTY-TRAY-FURROW

In state s_r^3, the robot travels inside a furrow - carrying an empty tray - toward the location where the transport request originated. The initial conditions are $\mathbf{X}_{r,0} = [\mathrm{x}_e, \mathrm{y}_e, W_{empty}, t]$. The robot speed is $V_{s_r^3} = V_r$, and the travel angle θ is the heading of the furrow with direction toward the position where the tray becomes full $(\mathrm{x}_b,\ \mathrm{y}_b)$; the picking rate is zero. The "*Picker location*" transition, s_r^3 to s_r^4, occurs once the robot arrives at the picker position (within a small fixed distance before it).

WAITING-FOR-PICKER

In state, s_r^4, the robot is idle and waits for the picker to finish. Depending on the operation scenario, if robots respond to requests the time spent in this state will be zero; however, if some form of predictive scheduling is performed, the robot may arrive early. The initial conditions are $\mathbf{X}_{r,0} = [\mathrm{x}_b, \mathrm{y}_b, W_{empty}, t]$, and the robot speed and picking rate are both zero. The "*Picker ready*" transition, s_r^4 to s_r^5, takes place when the picker's "*Tray full*" condition (and transition from s_p^4 to s_p^{10}) becomes true.

TRAY-LOADING
In state, s_r^5, the robot is idle, while a picker takes its empty tray and places a full tray on it. The initial conditions are $\mathbf{X}_{r,0} = [\mathrm{x}_b, \mathrm{y}_b, W_{empty}, t]$, and the robot speed is zero. The "handling time" for this state is assumed constant and equal to Δt_h. Tray handling is modeled with a picking rate $p_{s_r^4} = (W_{full} - W_{empty})/\Delta t_h$, which results in a fully loaded robot ($\mathrm{W}_{r,k} = W_{full}$) at the end of the state. The "*Full tray from picker*" transition, s_r^5 to s_r^6, takes place when the picker's "*Empty tray from robot*" condition ($T_{p,k} \geq t + \Delta t_h$) and corresponding transition becomes true.

TRANSP-FULL-TRAY-FURROW
In state s_r^6, the robot travels inside a furrow – carrying a full tray – toward the furrow's end-point. The initial conditions are $\mathbf{X}_{r,0} = [\mathrm{x}_b, \mathrm{y}_b, W_{full}, t]$, and the robot speed is $V_{s_r^5} = V_r$, and the travel angle θ is the heading of the furrow with direction toward the headland; the picking rate is zero. The "*End of furrow*" transition, s_r^6 to s_r^7, takes place reaches the end-point of the furrow $(\mathrm{x}_e, \mathrm{y}_e)$.

TRANSP-FULL-TRAY-HEADLAND
In state s_r^7, the robot travels in the headland – carrying a full tray – toward the collection station. The initial conditions are $\mathbf{X}_{r,0} = [\mathrm{x}_e, \mathrm{y}_e, W_{full}, t]$, the robot speed is $V_{s_r^6} = V_r$, and θ is defined by the furrow end-point and collection station point, with direction toward the furrow.; the picking rate is zero. The "Reached c*ollection station*" transition from s_r^7 to s_r^1, takes place once the robot reaches the collection station at $(\mathrm{x}_{cs}, \mathrm{y}_{cs})$.

STOP
In state s_r^8, the robot stops its operation, after all harvesting and transporting is done. The state initial conditions are $\mathbf{X}_{r,0} = [\mathrm{x}_{cs}, \mathrm{y}_{cs}, W_{empty}, \mathrm{t}]$ and the time clock stops .

4.3 DEVELOPMENT OF A ROBOT-AIDED HARVEST SIMULATOR

4.3.1 Simulation Platform Architecture

A simulator for manual and robot-aided strawberry harvesting was developed based on the hybrid system models presented above using the Python programing language. Figure 7 shows the simulator's architecture. The *Pickers Operation* module implements the picker hybrid model during manual or robot-aided harvesting. The *Robots Operation* module implements the hybrid model of the robots' operations. The picker and robot states and transport requests are fed to the *Robot Scheduler* module, which schedules robot operations and issues dispatching commands to the robots.

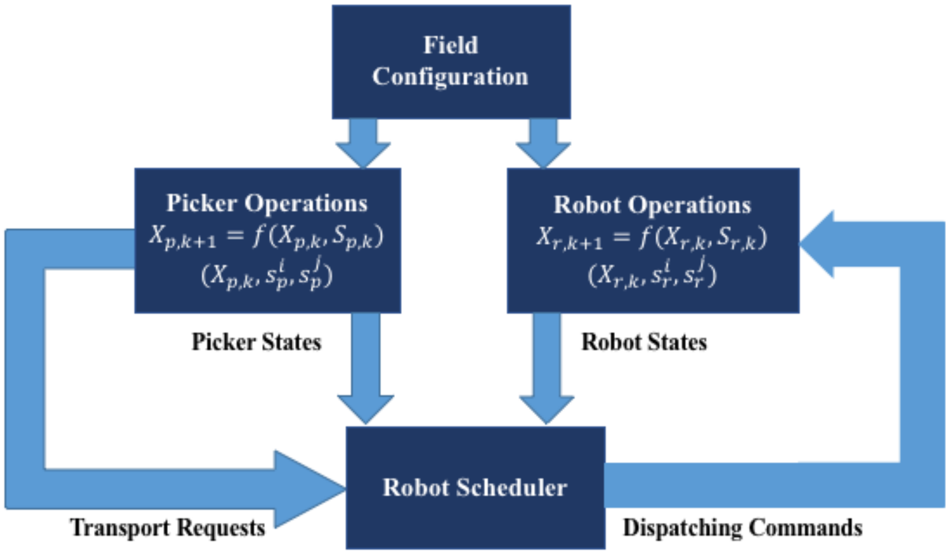

Figure 7. The architecture of the all-manual and robot-aided harvesting simulator. The picker and robot operations modules integrate the continuous picker and robot states $\boldsymbol{X_{p,k}}$ and $\boldsymbol{X_{r,k}}$ respectively, and execute the transitions of the respective discrete states, s_p^i and s_r^i.

The simulator has a global "clock", i.e., a global time variable, t, that represents the current time of the harvesting activity; time starts at $t = 0$ s and increases by Δt (0.5 s was used). The state updates are computed at every step and the simulation terminates when the entire field block is harvested, or after a pre-set harvest time has elapsed. During each execution of the simulator, the stochastic variables $V_P, V_T, V_W, \Delta t_{ef}$, and Δt_{iq} are sampled randomly from their respective non-parametric distributions. The random samples are stored, so that different scheduling algorithms can be compared for identical harvest conditions (yield, picker activity). A Monte-Carlo approach is adopted to estimate the mean harvest operation efficiency (Eq. 8). As a result, multiple runs of the harvest simulation are executed.

The simulation platform does not adopt a specific scheduling algorithm, as its purpose is to enable experimentation with various scheduling algorithms and optimization criteria. Instead, it defines the inputs and outputs of the *Robot Scheduler* module. The scheduler has access to the picker and robot continuous and discrete states, and to the set of all issued and yet-unserved tray transport requests at step k (each request contains its location and time). The output of the scheduler at step k, is the set of dispatching commands, where each dispatching command assigns a specific robot to a tray-transport location. For example, if only idle robots are dispatched, non-preemptive scheduling can be implemented; otherwise, if a robot that is on its way to an unserved request is assigned another request, preemptive scheduling can be performed. The scheduler module may contain a request prediction module, so that predictive scheduling is implemented; otherwise, reactive scheduling will be performed.

Figure 8 shows a visualization of simulated manual and robot-aided harvest with nine pickers and nine pickers and three robots respectively. In the manual harvesting mode (Figure 8a) as a picker fills up a tray (gold diamond), (s)he transports the filled tray to the active collection station (gold circle). Whereas, in the robot-aid harvesting mode (Figure 8b), as a picker fills up a tray, (s)he waits for a robot (colored circles) to arrive.

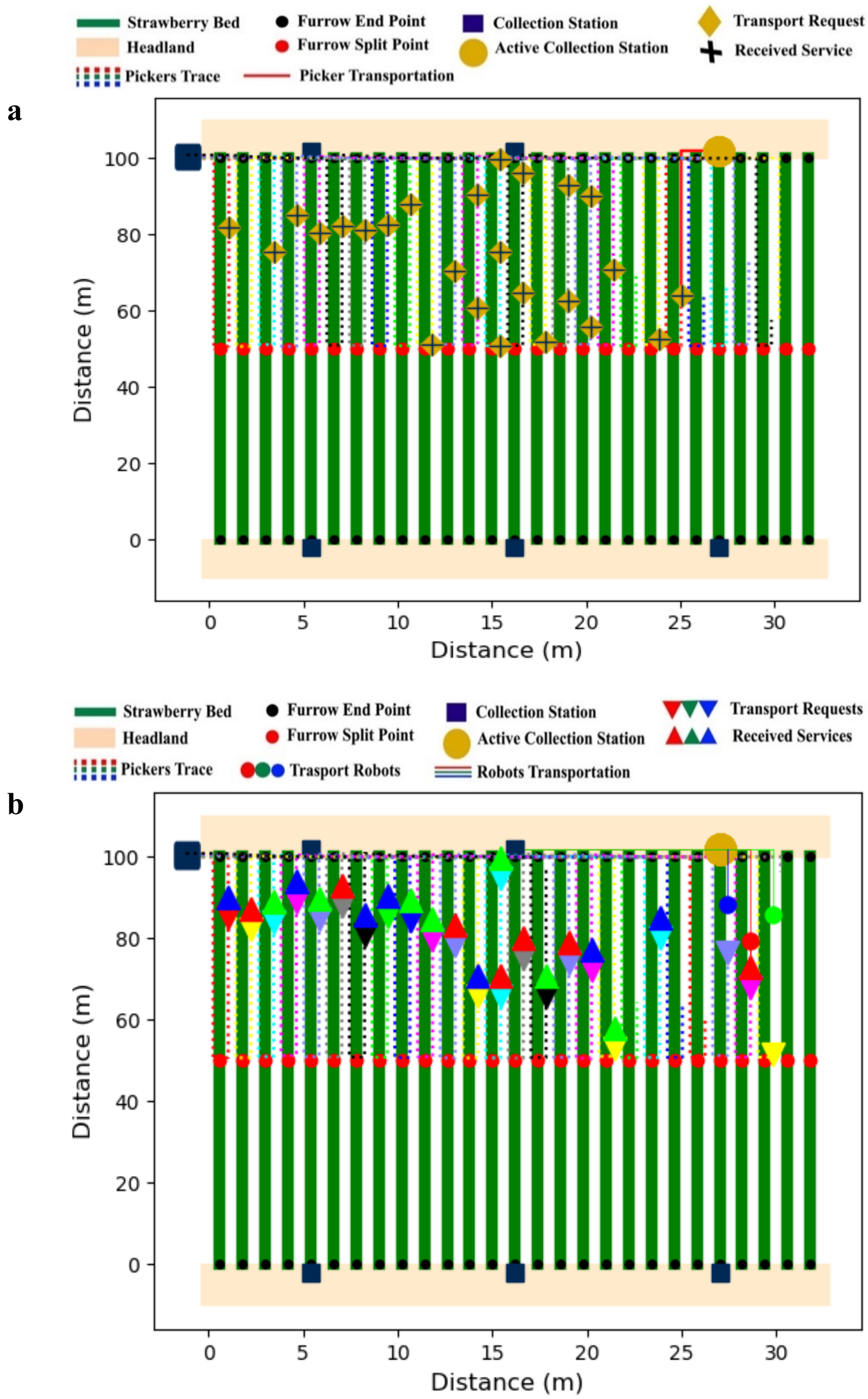

Figure 8. Snapshots of the simulator's visual outputs after 36 minutes of harvesting, in: a) manual harvesting mode, with nine pickers; b) robot-aided harvesting mode, with nine pickers and three robots. (Dimensions are not scaled for the purpose of illustration.)

4.3.2.3 Simulator Evaluation Metrics

Let the (productive) picking time required to fill an empty container be Δt_{ef}; also let the non-productive time be Δt_{fe} (due to picker's walking to the collection station, waiting in a queue, delivering harvested crops and receiving an empty container, and walking back to resume picking). If the size of the harvesting crew is P, and the number of containers harvested by picker i during a work shift is n_i, the harvest operation efficiency, $\overline{E}$, can be defined as the ratio of the sum of all productive times over the sum of all productive and non-productive times:

$$\overline{E} = \frac{\sum_{i=1}^{P}\sum_{j=1}^{n_i}\left(\Delta t_{ef}\right)_{ij}}{\sum_{i=1}^{P}\sum_{j=1}^{n_i}\left(\Delta t_{ef}\right)_{ij} + \sum_{i=1}^{P}\sum_{j=1}^{n_i}\left(\Delta t_{fe}\right)_{ij}} \tag{8}$$

The primary goal of the simulator is to predict the harvest operation efficiency, $\overline{E}$, under various operating scenarios. Since the distribution of Δt_{ef} is the result of measurements and it used (sampled) directly in the simulator, the actual metric of the simulator's performance must quantify how well Δt_{fe} is predicted. The simulator-predicted nonproductive time $\widehat{\Delta t}_{fe}$ is computed by summing the times spent in non-productive states, and is used as the simulator evaluation metric:

$$\widehat{\Delta t}_{fe} = \sum_{k=1}^{3} \Delta t_{s_p^k} + \sum_{k=7}^{8} \Delta t_{s_p^k} \tag{9}$$

5 Summary and Discussion

In this work, hybrid automata with stochastic parameters were used to model and simulate all-manual harvesting and machine aided harvesting using crop-transport robots. The discrete operating states of the pickers and robots, and their transitions and interactions, were modelled using finite state machines. The continuous states, including agent motions and mass transfer during both harvesting and tray-exchanges, were modeled using difference equations with stochastic parameters. Based on this methodology, a Monte-Carlo harvesting simulator was developed. The simulator samples the picker stochastic parameters and executes the hybrid automata which represents pickers, robots and their interactions. The robot scheduler module of the simulator enables the integration of various schedulers (such as reactive, pre-emptive, or predictive) for efficient robot dispatching.

The model and simulator can be used for the off-line evaluation of harvest-aid robots, by predicting the efficiency of harvest operations performed by a crew of human pickers and a team of crop-transport robots under various operating scenarios. Due to its foundation on hybrid automata, the model was developed to be used for harvesting simulation, but also to serve as an executable task model for robots to represent human actions, in the context of human-robot collaboration. The current model assumes that robots can carry only one tray, and hence must return to the collection station after serving one picker. This is not a structural limitation, and robot tray-carrying capacity can increase. The corresponding finite state machine would need to change slightly, so that the robot is dispatched to a new picker, until its tray carrying capacity is reached and it has to return to the collection station. The model and simulator were developed using commercial strawberry harvesting in mind; however, similar hybrid automata can be used to model manual and robot-aided harvesting in different settings, even with different crops – such as table grapes, tomatoes, blackberries - which are picked similarly to strawberries. The accompanying paper (Part II) of this work utilizes data gathered in two commercial strawberry fields during harvesting, to estimate the stochastic parameters involved in modeling pickers, and evaluate the prediction accuracy of the simulator for all-manual picking. Then, as a case study, the effects of different picker-robot ratios and priority-based reactive dispatching policies are reported on non-productive time and harvest efficiency.

6 Acknowledgements

This work is part of the National Robotics Initiative project titled "FRAIL-bots: Fragile cRop hArvest-aIding mobiLe robots" that was funded by NIFA-USDA Grant 11423498, and by NIFA Hatch/Multi-State Grant 1001069.

7 References

Anjom, F. K., et al. (2018). "Development of a linear mixed model to predict the picking time in strawberry harvesting processes." Biosystems Engineering 166: 76-89.

Ampatzidis, Y. G., Vougioukas, S. G., Whiting, M. D., & Zhang, Q. (2014). Applying the machine repair model to improve efficiency of harvesting fruit. *Biosystems Engineering, 120*, 25-33.

Arjona, E., Bueno, G., & Salazar, L. (2001). An activity simulation model for the analysis of the harvesting and transportation systems of a sugarcane plantation. *Computers and Electronics in Agriculture, 32*(3), 247-264.

Bac, C. W., Henten, E. J., Hemming, J., & Edan, Y. (2014). Harvesting Robots for High-value Crops: State-of-the-art Review and Challenges Ahead. *Journal of Field Robotics, 31*(6), 888-911.

Bechar, A., Yosef, S., Netanyahu, S., & Edan, Y. (2007). Improvement of work methods in tomato greenhouses using simulation. *Transactions of the ASABE, 50*(2), 331-338.

Bloomberg News. (2018). Farm Worker Shortage in EU. *Farm Journal*.

Bochtis, D., & Sørensen, C. G. (2010). The vehicle routing problem in field logistics: Part II. *Biosystems Engineering, 105*(2), 180-188.

Bochtis, D., Vougioukas, S., Ampatzidis, Y., & Tsatsarelis, C. (2007). Field operations planning for agricultural vehicles: A hierarchical modeling framework. *Agricultural Engineering International: CIGR Journal*.

Bochtis, D., Vougioukas, S., & Griepentrog, H. W. (2009). A mission planner for an autonomous tractor. *Transactions of the ASABE, 52*(5), 1429-1440.

De Toro, A., & Hansson, P.-A. (2004). Analysis of field machinery performance based on daily soil workability status using discrete event simulation or on average workday probability. *Agricultural systems, 79*(1), 109-129.

Elkoby, Z., van't Ooster, B., & Edan, Y. (2014). *Simulation Analysis of Sweet Pepper Harvesting Operations.* Paper presented at the IFIP International Conference on Advances in Production Management Systems.

Guan, S., Nakamura, M., Shikanai, T., & Okazaki, T. (2008). Hybrid Petri nets modeling for farm work flow. *Computers and Electronics in Agriculture, 62*(2), 149-158.

Guan, Z., Wu, F., Roka, F., & Whidden, A. (2015). Agricultural labor and immigration reform. *Choices, 30*(4), 1-9.

Hameed, I., Bochtis, D., Sørensen, C., & Vougioukas, S. (2012). An object-oriented model for simulating agricultural in-field machinery activities. *Computers and Electronics in Agriculture, 81*, 24-32.

Mesabbah, M., Mahfouz, A., Ragab, M. A., & Arisha, A. (2016). *Hybrid modeling for vineyard harvesting operations.* Paper presented at the Proceedings of the 2016 Winter Simulation Conference.

Seyyedhasani, H., & Dvorak, J. S. (2017). Using the Vehicle Routing Problem to reduce field completion times with multiple machines. *Computers and Electronics in Agriculture, 134*, 142-150.

Silwal, A., Davidson, J. R., Karkee, M., Mo, C., Zhang, Q., & Lewis, K. (2017). Design, integration, and field evaluation of a robotic apple harvester. *Journal of Field Robotics, 34*(6), 1140-1159.

Van't Ooster, A., Bontsema, J., van Henten, E. J., & Hemming, S. (2012). GWorkS–A discrete event simulation model on crop handling processes in a mobile rose cultivation system. *Biosystems Engineering, 112*(2), 108-120.

van't Ooster, A., Bontsema, J., van Henten, E. J., & Hemming, S. (2015). Model-based analysis of skill oriented labour management in a multi-operations and multi-worker static cut rose cultivation system. *Biosystems Engineering, 135*, 87-102.

Van Henten, E. J., Bac, C., Hemming, J., & Edan, Y. (2013). Robotics in protected cultivation. *IFAC Proceedings Volumes, 46*(18), 170-177.

Vougioukas, S. G., Spanomitros, Y., & Slaughter, D. (2012). *Dispatching and routing of robotic crop-transport aids for fruit pickers using mixed integer programming.* Paper presented at the 2012 Dallas, Texas, July 29-August 1, 2012.

Williams, H.A., Jones, M.H., Nejati, M., Seabright, M.J., Bell, J., Penhall, N.D., Barnett, J.J., Duke, M.D., Scarfe, A.J., Ahn, H.S. and Lim, J., 2019. Robotic kiwifruit harvesting using machine vision, convolutional neural networks, and robotic arms. biosystems engineering, 181, pp.140-156.

Zhou, K., Jensen, A. L., Bochtis, D. D., & Sørensen, C. G. (2015). Simulation model for the sequential in-field machinery operations in a potato production system. *Computers and Electronics in Agriculture, 116*, 173-186.